NIST Author Manuscript

NIST Author Manuscript

NIST Author Manuscript

Author Manuscript
Accepted for publication in a peer-reviewed journal

NIST National Institute of Standards and Technology • U.S. Department of Commerce

Published in final edited form as:
J Manuf Sci Eng. 2019 ; 141: . doi:10.1115/1.4042789.

A Review of Model Inaccuracy and Parameter Uncertainty in Laser Powder Bed Fusion Models and Simulations

Tesfaye Moges[1],
Engineering Laboratory, National Institute of Standards and Technology, Gaithersburg, MD 20899

Gaurav Ameta, and
Engineering Laboratory, National Institute of Standards and Technology, Gaithersburg, MD 20899

Paul Witherell
Engineering Laboratory, National Institute of Standards and Technology, Gaithersburg, MD 20899

Abstract

This paper presents a comprehensive review on the sources of model inaccuracy and parameter uncertainty in metal laser powder bed fusion (L-PBF) process. Metal additive manufacturing (AM) involves multiple physical phenomena and parameters that potentially affect the quality of the final part. To capture the dynamics and complexity of heat and phase transformations that exist in the metal L-PBF process, computational models and simulations ranging from low to high fidelity have been developed. Since it is difficult to incorporate all the physical phenomena encountered in the L-PBF process, computational models rely on assumptions that may neglect or simplify some physics of the process. Modeling assumptions and uncertainty play significant role in the predictive accuracy of such L-PBF models. In this study, sources of modeling inaccuracy at different stages of the process from powder bed formation to melting and solidification are reviewed. The sources of parameter uncertainty related to material properties and process parameters are also reviewed. The aim of this review is to support the development of an approach to quantify these sources of uncertainty in L-PBF models in the future. The quantification of uncertainty sources is necessary for understanding the tradeoffs in model fidelity and guiding the selection of a model suitable for its intended purpose.

Keywords

additive manufacturing; powder bed fusion; model uncertainty; parameter uncertainty; uncertainty quantification

1 Introduction

Additive manufacturing (AM) is a process of producing parts by depositing material layer by layer without part-specific tooling based on a 3D part model [1]. Among the different AM

[1]Corresponding author. tesfaye.moges@nist.gov.

This material is declared a work of the U.S. Government and is not subject to copyright protection in the United States. Approved for public release; distribution is unlimited.

NIST Author Manuscript NIST Author Manuscript NIST Author Manuscript

processes, powder bed fusion (PBF) is often referred to as the most promising technology capable of manufacturing complex geometry of metallic parts applicable in aerospace, automotive, marine industries, and biomedical implants [2–7]. The two main processes of PBF are selective laser melting (SLM) and electron beam melting (EBM). The operating principle of the PBF process is that a thin layer of powder material is applied on a build platform, and an energy source (laser or electron beam) is employed to selectively scan and fuse the powder particles as per the desired geometry. After one layer is completed, the build platform is lowered by the prescribed layer thickness and an additional powder layer is spread. This process is repeated until building of the part is completed [8]. When a powder bed is used in the SLM process, it is specifically called laser powder bed fusion (L-PBF) process.

The L-PBF technology has many advantages compared to conventional manufacturing methods. The L-PBF technology produces parts having complex geometry and internal structures, sometimes without the need of support structures, from a wide range of engineering materials such as polymers, ceramics, and metals [9] while reducing lead time, minimizing material wastage, and producing nearly full-dense final parts [5,10]. In addition, L-PBF has the ability to tune properties during the processing of the parts and can produce near-net-shaped components ready to use [11]. Although the L-PBF process is a promising technology, it faces challenges when creating parts with consistent quality in terms of mechanical properties, surface finish, and fatigue life. Some of these challenges can be attributed to the existence of unstable fusion, thermal gradients, and process variabilities [12] that have not been fully understood [13].

To overcome these challenges, intensive experimental investigations continue, but these studies are time consuming and costly. Research efforts are also devoted to the development of predictive computational models and simulations to understand the dynamics and complexity of heat and phase transformations [14–16]. Although computational models and simulations are promising tools to understand the physics of the process, the lack of quantitative representation of their prediction accuracy hinders further application in process control and optimization. Due to this reason, it is very challenging to select suitable models for the intended purpose. Therefore, it is important to study and investigate the degree of accuracy and uncertainty associated with L-PBF models.

The focus of this paper is to review existing L-PBF models, their assumptions, and associated uncertainties. The rest of the paper is organized as follows: Sec. 2 presents the basics of L-PBF process and the summary of previously published review papers. Section 3 presents a review of different models in L-PBF with associated modeling assumptions. Parameter uncertainty is discussed in Sec. 4, which is followed by a discussion of uncertainty quantification (UQ) related challenges in Sec. 5. Section 6 presents some conclusive remarks, including future directions on uncertainty quantification.

NIST Author Manuscript

NIST Author Manuscript

NIST Author Manuscript

2 Background

2.1 Physical Phenomena in L-PBF Process.

A simple overview of the L-PBF process is shown in Fig. 1. Due to the inherent nature of L-PBF process, the powder particles experience rapid heating, melting, and solidification processes within a short period of time. Thus, dynamics and complex physical phenomena occur during the process over a broad range of time and length scales at different phases of the process from powder layer formation to melting and solidification [17,18]. The melt pool dynamics that occur during the process include the convective flow of molten metal driven by Marangoni effect due to the surface tension gradient on the top surface of the molten pool and the effect of recoil pressure of the expanding vapor and evaporation losses [19,20]. This process is governed by a variety of physical mechanisms, such as heat source–particle interaction, powder layer formation, heat transfer, fluid dynamics of the molten pool, and phase transformations.

The physics often modeled in the L-PBF process can be characterized by five physical phenomena. First is the powder layer deposition. In this step, powder particles of different size get pushed by a re-coater onto the last layer in the build chamber due to gravity, friction, and other forces among the powder particles. Second is the delivery of laser energy onto the powder. Laser energy, guided by the optics and galvanometer, is directed to the appropriate location on the powder layer. Here, the laser energy interacts with the powder and gets converted into the heat energy. Third is the formation of the melt pool. In this step, the heat energy from a moving laser melts the powder and forms a melt pool with a transient temperature field around it. Fourth is the solidification of the melt pool due to heat dissipation. Fifth is the development of residual stress due to different heating and cooling rates across multiple layers and within a layer. All these physical phenomena are depicted in Fig. 1, with various L-PBF process parameters.

2.2 Summary of Previous Reviews.

The five physical phenomena are often only partially addressed. The predictive accuracies of L-PBF models of the five physical phenomena are affected by modeling assumptions, numerical accuracy, parameters uncertainty, and measurement uncertainty for validation. To better understand the uncertainties and inaccuracies of these models, several researchers have reviewed the L-PBF modeling literature [21]. Although several reviews of L-PBF models exist in the literature, the sources of uncertainty and inaccuracy are not explicitly considered.

Assouroko et al. [21] studied the heat absorption and melt pool models to identify the model inputs and the underlying physics of the L-PBF models. They did not consider all the associated assumptions and did not review the sources of parameter uncertainties. Roh et al. [22] reviewed an additional solidification model, but did not consider the sources of parameter uncertainties. Witherell et al. [23] reviewed additional model, but did not review the sources of parameter uncertainties. Hu and Mahadevan [24] reviewed all five models, but a comprehensive review of their assumptions and the sources of parameter uncertainty is still

NIST Author Manuscript NIST Author Manuscript NIST Author Manuscript

lacking. These studies reviewed some of the L-PBF models without considering the sources of inaccuracy and uncertainty associated with modeling assumptions and input parameters.

Lopez et al. [25] conducted the uncertainty quantification in an L-PBF model to quantify model uncertainty considering the melt pool model as a case study. They used the melt pool model to characterize uncertainty in the melt pool dimensions based on certain assumed uncertainties in the input parameters of the melt pool model. Furthermore, the uncertainty quantification included numerical uncertainty and measurement uncertainty.

The predictive accuracy of L-PBF models strongly depends on the included and neglected physics of the process. *Modeling inaccuracy* originates from the modeling assumptions that neglect the part of the physical phenomena of a process. In addition, computational models require several input parameters including process parameters and material properties to represent the physical scenario of the process. However, the value of some parameters cannot always be known precisely and may exhibit inherent temporal fluctuations. Therefore, there is an associated *parameter uncertainty* in the computational models due to unknown input parameters. Moreover, the mathematical equations used to formulate the physical phenomena are difficult to be solved analytically, and various numerical methods have been used to discretize the system into finite elements and temporal transient phenomena into time-steps to obtain an approximate solution. This discretization introduces *numerical uncertainty* in the computational models. Finally, to validate the simulation results against measurement data, experimental results introduce *measurement uncertainty* due to imprecise measurement methods. Therefore, modeling uncertainty includes parameter uncertainty, numerical uncertainty, and measurement uncertainty for validation [26].

In general, model assumptions lead to inaccuracies in model predictions. Prediction uncertainty arises due to model uncertainty, which includes parameter uncertainties, numerical accuracy, and measurement uncertainty. Usually, L-PBF simulation models have several variables that cannot be experimentally measured. The values of these variables are estimated by calibrating the model output with experimental outcomes [27,28]. Model predictions are affected by both inaccuracy and uncertainty. Model inaccuracy arises from modeling assumptions, while model uncertainty is a resultant of various sources of uncertainties combined within the model.

It is critical to review and consider all the phenomena and their modeling assumptions and sources of parameter uncertainty to quantify uncertainties in the L-PBF models. The modeling inaccuracy and parameter uncertainty sources are discussed in Secs. 3 and 4, respectively.

3 Sources of Model Inaccuracy

The accuracy of computational models and simulations strongly depends on the included and neglected physics of the process. Modeling inaccuracy originates from the modeling assumptions that neglect the part of the physical phenomena of a process [25,29]. In this section, we focus on metal L-PBF process and discuss some of the common sources of

NIST Author Manuscript

NIST Author Manuscript

NIST Author Manuscript

modeling inaccuracies due to modeling assumptions that exist in powder, heat source, melt pool, solidification, and residual stress models.

3.1 Powder Bed Models.

The L-PBF process begins with the formation of a powder layer on a substrate. The packing structure, which is the output of powder bed models, is dependent on parameters such as powder size and shape, particle size distribution, layer thickness, and re-coater shape. The powder bed is formed when the powder delivery piston rises, the build platform lowers by the predefined layer thickness, and the re-coater moves forward and spreads a layer of particles on the build platform. In addition to the powder bed parameters, the re-coater velocity also influences the surface structure and packing density of the powder bed [30,31]. During the powder bed formation, a number of phenomena such as *friction*, *collision*, and *adhesion* occur due to the interaction among microsized particles. As a result, different forces, such as *elastic*, *frictional forces*, *gravity*, and *van der Waal forces*, can influence powder bed morphology [32–34].

To simulate the powder bed formation in L-PBF, several numerical models have been proposed based on the discrete element method (DEM) or the Raindrop packing algorithm. In DEM, inter-particle forces computed using nonlinear Hertz theory are explicitly considered [32–36]. The Raindrop packing algorithm randomly deposits powder particles without considering interaction forces among particles [37–40]. Figure 2 depicts the input, output, and characteristics of the two types of models.

Moreover, in numerical simulations of the powder bed, considering the particle size distribution as a Gaussian (most common) [32,33,41], bimodal (provides higher powder packing density) [33,39,41], uniform (less common) [32], or monosized (ideal condition) [32,33,39] distribution significantly affects the powder bed morphology. Each distribution type provides different packing density and porosity of the powder bed, especially at small layer thickness [33]. The choice of particle size distribution has a significant influence on factors that directly depend on the packing density like the value and degree of fluctuations of absorptivity of powder bed [41] and radiative transfer process [42].

In most of the powder bed simulations, the shape of the particle is assumed to be spherical. However, the particles are of complex geometrical shape that significantly alters the packing nature and size distribution of the powder bed [31]. In addition, while recycling powder particles, oxygen content increases leading to changes in particle size distribution, shape (distortion), and surface roughness [43]. Moreover, when the powder size is relatively small, the effect of van der Waal forces becomes significant, and the particles have the tendency to agglomerate together. This causes the flow-ability of the powder to reduce, which results in poor estimation of powder bed density (packing density) [44].

Thus, neglecting these factors and simplifications and assumptions related to interaction between particles causes model inaccuracies in powder bed models.

NIST Author Manuscript NIST Author Manuscript NIST Author Manuscript

3.2 Heat Source Models.

Once the powder bed is formed, thermal energy in the form of a laser beam is applied on the powder bed, as per the scanning strategy, to melt and fuse particles together. The amount of heat absorbed by the powder bed is governed by many factors, such as laser power, beam spot size, thermal conductivity of a material, powder size and shape, size distribution, packing density, surface oxidation, and contamination [16,41]. Based on the intensity of laser power distribution on the surface of the powder bed, the heat source is assumed to be (a) a point heat source that discards the diameter of the laser beam spot [45,46], (b) a cylindrical heat source that assumes the uniform intensity within the spot size [21], (c) an ellipsoidal heat source that assumes the heat intensity decays exponentially with distance from the center of the source [47–49], or (d) a Gaussian heat source that considers the intensity of power to be a normal distribution [50]. When the laser beam strikes the powder bed, multiple scattering of laser rays occurs within the powder particles and in the melt pool [15], and hence, the penetration depth is comparable to the layer thickness [51]. Multiple scattering of the laser beam causes the absorptivity of the powder bed to be higher than the absorptivity of laser on a flat surface [41,52]. Thus, assuming the absorbed energy to be constrained on the surface instead of the volume of the powder bed considerably reduces the predictive accuracy of the heat source model [53].

To determine the amount of absorbed energy and absorptivity of the powder bed, a number of numerical models are developed on the basis of (a) a radiation transfer formulation that derived analytical solution from a homogeneous continuum radiation transfer equation (RTE) using powder porosity and surface areas [51], (b) a ray tracing method that accounts for the effect of multiple reflections by tracking the trajectories of each photon [41,54], and(c) a Beer–Lambert approach that assumes the laser beam is predominantly absorbed at the powder surface of the first incidence layer and relates attenuation of irradiation intensity with penetration depth as a function of exponential decay [55–57]. Considering their varying assumptions, these heat source models intrinsically carry significant inaccuracy that further propagates into the subsequent melt pool and solidification models [24]. Table 1 presents the inputs, outputs, and characteristics of these different models.

Moreover, due to the moving nature of the heat source in L-PBF process, the thermal diffusion time is short, resulting in partial melting of the particle and possibly causing defects in the form of pores or inclusions in the finished part [41]. Thus, while modeling the heat source in the L-PBF process, it is important to consider the powder bed as a distribution of interacting powder particles instead of idealizing it as a continuum material. Treating the powder bed as a continuum body ignores the effect of several physical phenomena induced by fluid dynamics, such as surface tension and wetting, that are present in the molten pool [52,60]. Therefore, assumptions associated with the distribution of absorbed energy (surface versus volumetric) and powder bed material (continuum versus powder particles) potentially govern the fidelity of the heat source models. A model that considers simplified assumptions and neglects realistic characteristics of the powder bed possess a substantial amount of modeling inaccuracy.

NIST Author Manuscript

NIST Author Manuscript

NIST Author Manuscript

3.3 Melt Pool Models.

The absorbed heat energy from the laser beam is locally dissipated across the powder bed, and when the powder reaches its melting temperature, a melt pool is formed, and consolidation of particles occurs at locations exposed directly to the laser power. Consolidation of molten particles, melt pool dynamics, and melt pool characteristics, such as melt pool shape and dimensions (width, depth, and length) and the temperature gradient, are affected by different factors and phenomena that exist in the process. These factors include the surface tension of melt pool, capillary and Marangoni forces, wetting behavior of the melt pool, Plateau–Rayleigh instability, viscosity of the molten pool, gravity, shrinkage, inertia effect, surrounding atmospheric pressure, evaporation, recoil pressure, buoyancy force, spattering, heat convection and radiation, and layer thickness of the powder bed [52,55,60–62].

The accuracy of predictive melt pool models significantly depends on the incorporation of these factors. Since temperature-dependent surface tension governs the flow of the melt pool from hot to cold regions, which causes Marangoni convection transfer, surface tension influences the surface quality and morphology of the track formation [37,63,64]. When the surface tension effect is considered in a melt pool model, the binding of melted particles together and the formation of smoother surface due to an increase in contact area with the substrate are better captured [65]. The wetting behavior of the melt pool with the substrate or previous layers and surrounding powder particles due to surface tension strongly affects the shape of the melt pool and continuity as well as adhesion to the previous layer [52]. The presence of factors, such as surface roughness of powder particles, oxidation, and contamination in powder bed, cause improper wetting, which results in the formation of defects such as balling, pores, uneven surface, and delamination between layers [66]. The evaporation phenomenon occurs when the temperature of the melt pool exceeds the boiling point especially at high energy density. The resulting loss of mass and additional cooling induce recoil pressure on the melt pool, which possibly leads to the formation of keyhole-related defects [67–70]. Thus, for better understanding of the melt pool dynamics at high heat intensity, the effect of evaporation phenomena should be considered [71].

Direct measurement of complex melt pool mechanisms has been extremely cumbersome and time consuming [72]. Therefore, computational models and simulations that consider the physical phenomena occurring during the process are developed. For quick prediction of the temperature field of a track and melt pool geometry, highly simplified thermal models [45] based on Rosenthal’s approach [46] have been developed for L-PBF process [25]. Although these models provide quick and preliminary results that can be starting points for the development of numerical models [21], several physical phenomena, such as phase changes, melt pool flow, powder particle packing, and energy distribution, are neglected. Therefore, to (a) better understand and capture the complex physical phenomena of the melt pool, (b) simulate the melt pool dynamics, and (c) determine melt pool characteristics and thermal history of a track, several numerical models have been developed based on different approaches.

The finite element method (FEM)–based thermal model is the most popular approach for simulating L-PBF process and predicting temperature field and melt pool characteristics

NIST Author Manuscript NIST Author Manuscript NIST Author Manuscript

[15,73]. In this approach, the powder bed and substrate are discretized into finite number of elements to solve heat transfer governing equations and boundary conditions. Considering (a) convection heat loss due to surrounding gas, (b) thermal radiation loss on the free surface, (c) temperature-dependent material properties, and (d) the effect of latent heat of fusion during phase changes, certainly improve the predictive accuracy of FEM-based thermal models [50,57,74–77]. The common assumptions of FEM thermal models are that the powder bed is considered to be a continuum body instead of randomly distributed particles, and the dynamics of the melt pool, including fluid flow and convection of the melt pool due to surface tension, are neglected. These simplifications can potentially cause significant modeling inaccuracy when estimating melt pool characteristics and the temperature field of the track where the laser scanning occurs.

To understand the dynamics in melt pool formation, a number of numerical models have been developed based on (a) the Lattice Boltzmann method (LBM) and (b) computational fluid dynamics (CFD)–based models. LBM uses particle collusion and considers the hydrodynamics effects in the melt pool [13,20,37,56,78]. The CFD models include (a) finite difference method (FDM) and volume of fluid (VOF) method used to track the free surface of the molten pool and Flow-3D code to solve the governing equations [79], and (b) finite volume method (FVM) with VOF to solve mass, momentum, and energy conservation equations using tools, such as OpenFOAM and Flow-3D [63,80–85]. In addition, coupling FEM and FVM using ALE3D code by utilizing arbitrary Lagrangian–Eulerian techniques is another numerical method used for melt pool model [64,65]. Since these methods consider the powder bed to be a distribution of particles and partially or fully incorporate the physical phenomena mentioned above, they provide better predictive accuracy than FEM and Rosenthal-based thermal models. It should be noted that neglecting some of the factors mentioned above introduces inaccuracy associated with modeling assumptions that affect the model fidelity [86]. The inputs, outputs, and characteristics of these melt pool models are listed in Table 2.

As mentioned above, the L-PBF melt pool possesses many physical phenomena that need to be considered while predicting melt pool shape and geometry, thermal history of a track, defects such as balling, porosity, and delamination between layers. The model assumptions potentially affect the fidelity of the predictive models and result in modeling inaccuracy.

3.4 Solidification Models.

When the heat source moves away from a certain location in a powder bed, the molten material becomes cool and starts to solidify, and the evolution of grain structure begins. The microstructure characteristics such as grain size, grain morphology, and grain texture are required for predicting the mechanical properties of the final part [60]. The temperature gradient obtained from the melt pool model and cooling rates induced by the scanning speed of the laser beam are the main input variables that govern the evolution of grain structure during the solidification process [98]. In addition, melt pool dimensions also have influence on the characteristics of microstructure. It is observed that the cross-sectional area of the melt pool affects the grain size, whereas the melt pool area-to-depth ratio influences the grain morphology during solidification [99]. Due to the moving nature of the heat source,

NIST Author Manuscript NIST Author Manuscript NIST Author Manuscript

the molten pool experiences rapid cooling and fast solidification, which result in fine grain formation and thus good mechanical properties [100]. The previous layers and adjacent tracks are exposed to heat treatment and experience repeated heating and cooling cycles. The thermal gradients and cooling rates that influence the characteristics of microstructure depend on scanning speed, scanning strategy, hatch distance, material properties, part geometry, build time, build direction, temperature of the build platform, part porosity, and grain size distribution [52,101–103]. The fidelity of a solidification model that predicts the metallurgical microstructure of the produced part depends on the accuracy of the temperature gradients of the locations directly exposed to the heat source and other affected locations (i.e., previous layers and adjacent scan tracks) that are influenced by different physical phenomena as discussed in Sec. 3.3.

Modeling the solidification process to determine the evolution of microstructure in L-PBF is important as it helps for the accurate prediction of residual stresses and distortion. Since the solidification process utilizes the thermal history of the melt pool in the heat-affected zone and locations at previous layers and adjacent scan tracks, it needs to be coupled with the melt pool model. To study the solidification process and simulate the evolution of grain structures, the phase field (PF) method and cellular automata (CA) approaches are commonly used [104].

The formulation of the PF model [105–108] is based on the free energy function and explicitly considers the locations of liquid, solid, and liquid–solid phase boundaries. It is coupled with a FEM-based thermal model of the melt pool that provides the temperature field to study the solidification process. The CA approach [101,108–111] geometrically tracks the grain growth in the heat-affected zone. To simulate the evolution of grain growth in the solidification process, the CA approach is coupled with melt pool models, such as LBM [111] and FDM [101]. The CA model is also coupled with the FEM-based thermal model to simulate micro-structure evolution and to study the contributions of variability in several parameters to grain size distribution [96,110,112]. Since microstructure evolution approaches simulate solidification process on the basis of different assumptions and approximations, there is associated model inaccuracy that affects the accurate prediction of the microstructure characteristics and metallurgical properties. The inputs, outputs, and characteristics of these different solidification models are presented in Fig. 3.

3.5 Residual Stress Models.

Due to high thermal gradients near the laser spot and the surrounding area, rapid cooling when the laser moves, and repeated heating and cooling cycles, the material experiences successive thermal expansion and shrinkage to produce localized compression and tension that induce residual stresses in the produced part [102]. These thermally induced residual stresses partially relax when the support structures and surrounding powders are removed. Depending on part geometry, they may cause fatigue crack growth and deformation in the final part, which may result in warping, loss of edge tolerance, loss of net shape, and part failure [102,113,114]. The residual stresses and distortion of the produced part are potentially affected by the build orientation, scanning strategy, and preheating of the build platform [115,116]. To mitigate residual stresses, some of the applied techniques are proper

NIST Author Manuscript NIST Author Manuscript NIST Author Manuscript

selection of scan strategies and build orientation [117,118], in situ heating of the powder bed [119], and ex situ heat treatment before removing support structures [120]. In addition, since larger residual stresses are observed at the top layer and substrate–part connection [121], filleting the edges can reduce stress concentration at these regions [122]. Thus, to simulate the residual stresses and distortion, which is commonly performed at part scale, it is necessary to consider the effect of support structures, surrounding powder particles, and the build platform [60].

A simplified mathematical model is derived to predict the general profile of residual stresses using equilibria of force and moment as per the general beam theory based on a number of assumptions [116]. However, the most common residual stresses prediction method in the L-PBF process is the thermomechanical FEM-based analysis that uses the temperature gradients determined from the melt pool model as thermal loading [123,124]. In addition to the temperature history, the characteristics of microstructure determined from the solidification model are also used as input to residual stress models. These are used to perform elastoplastic mechanical analysis for the computation of residual stress and distortion [125]. In FEM-based analysis, the material deposition is modeled by using *quiet* element or *inactive* element activation approaches, which are activated as the added material solidifies [49]. In the *quiet* element activation approach, the elements are present from the start of the analysis, but due to their assigned properties, they do not affect the analysis. However, in the *inactive* element activation approach, the elements are not included in the analysis until the corresponding material is added [125]. To include phase transformation phenomena for predicting residual stresses and distortion, FEM analysis uses these activation approaches, also known as element birth and death in ABAQUS and ANSYS [15]. These elements are deactivated until solidification is completed, and then they are activated back to attain their actual stiffness [15]. The residual stress and distortion are predicted by utilizing a thermoelasto-plastic constitutive material model that can be solved using CUBIC code by Pan Computing LLC (Autodesk Inc.), which includes the stress relaxation effect due to annealing [122]. Moreover, thermomechanical FEM analysis is utilized to predict the residual stresses and distortion occurring during the cooling cycle [121]. The inputs, outputs, and characteristics of these different residual stress models are presented in Fig. 4.

The prediction accuracy of residual stress and distortion strongly depends on the factors considered in the material constitutive model, such as material inhomogeneity and anisotropy, temperature field, microstructure, and temperature-dependent mechanical properties of the material. Thus, the inaccuracies present in the melt pool and solidification models propagate to residual stress and distortion models via temperature history and microstructure characteristics.

4 Sources of Parameter Uncertainty

Due to the complexity of the L-PBF process, more than 130 parameters affect the quality of the final part [126]. Since precise values of some of these parameters are not known, computational models can have uncertainty due to unknown values of the input parameters. In addition, due to inherent temporal fluctuations and variation in input parameters, such as laser power, scan speed, powder size, powder shape, and powder size distribution, there is

NIST Author Manuscript

NIST Author Manuscript

NIST Author Manuscript

uncertainty associated with these parameters that reduce predictive accuracy of a model. Some of the sources of uncertainty related to input parameters that affect the accuracy of the L-PBF models are discussed in this section.

4.1 Layer Thickness.

Layer thickness is the quantity that describes the predetermined thickness of the powder layer for each layer of scanning [127]. It is one of the main controllable process parameters that is directly correlated with the quality of the part and its effects have been studied in Refs. [128–132]. The accuracy of the powder bed layer thickness depends on (a) motion and position of build platform and re-coater arm [133] and (b) powder bed density. The density of the powder bed affects the layer thickness, and due to consolidation of the powder, the *effective layer thickness* is different from the nominal value. The effective layer thickness is the nominal layer thickness divided by the powder packing density [13,134]. Although the re-coater spreads approximately the same amount of material in one layer, the density of the powder packing is not the same [93]. As a result, variation in powder bed density causes layer thickness of the powder bed to inherit uncertainty. Based on the review of literature, the sources of uncertainties in layer thickness can be categorized as uncertainties related to build platform motion, powder bed density, and re-coater arm motion.

4.2 Laser Power.

Laser power is the rate at which energy is emitted from a laser. It is one of the most critical controllable parameters that has an impact on the quality of the finished part and influences the consolidation process. Uncertainty in the laser power arises due to (a) inherent drift in the Galvanometer control system [135,136], (b) heating of optics, and (c) soot on optics. When various components of the beam delivery optics within the laser path heat up, it can potentially cause loss of power on the build plane. Moreover, during the L-PBF process, the build chamber gets dirty, and soot can accumulate on beam delivery optics and block the laser path. This contamination effectively reduces the laser power at the build plane, and when the contaminated optics heat up, it can further reduce the laser power.

There are dynamic effects that limit the accuracy of the laser power, scan speed, and laser spot position due to disturbance of the laser and galvo systems during switch on and off. Laser systems require time to reach a normally steady state in which it exhibits small oscillations as output power does not immediately attain its steady state [137]. In other words, when the laser is suddenly switched on, the laser emits a number of spikes and undergoes damped relaxation oscillations before the steady state is reached [138]. Because of laser power fluctuation, perturbation during the melting process can be observed and uniform melt pool dimensions could not be achieved [139]. Based on the review of literature, the source of uncertainties in laser power can be categorized into galvanometer system and optics system.

4.3 Laser Scan Speed.

Scan speed is another critical controllable parameter that decides the quality of the produced part as it influences the melting and solidification processes [139]. Uncertainty in scanning speed arises from (a) Galvanometer’s inherent drift and intrinsic error [140] and (b) heating

NIST Author Manuscript

NIST Author Manuscript

NIST Author Manuscript

and intrinsic errors in positioning optics [140,141]. The dynamic effects of the galvo system depend on the input frequency, acceleration, and other related factors. Small variations in scanning speed perturb the melting process and result in a noticeable effect on peak temperature and melt pool geometry [142].

Based on the review of literature, the source of uncertainties in laser scan speed can be categorized into galvanometer and optics systems. Figure 5 shows uncertainty sources in a fishbone diagram highlighting the factors that affect layer thickness, laser power, and scan speed.

4.4 Absorptivity.

Absorptivity is the ratio of the optical power absorbed by the material to the incident power applied [143]. Absorptivity depends on powder material, particle shape and size, distribution of particle sizes, porosity, layer thickness, and laser beam size, wavelength, and profile [16,41]. Due to multiple scattering of light, when the laser strikes the powder, the absorption is significantly larger than its value from normal incidence on a flat surface. During keyhole formation, multiple reflections of laser light directly strike the keyhole wall, resulting in an increase in the energy transfer from the laser to the material and increases absorption [144,145].

Although direct measurement of absorption is very difficult [146], it is important to capture the realistic aspects affecting the absorptivity of the powder [143,146]. These aspects include nonspherical particle shape, real powder structure, surface oxidation, alloy materials, and surface roughness of the powder [16,143,147,148]. Therefore, these factors result in significant uncertainty in the absorption coefficient of the powder bed in L-PBF process. Based on the review of literature, the source of uncertainties in powder bed absorptivity can be categorized as uncertainties related to powder properties, material properties, effective layer thickness, and laser beam properties.

4.5 Temperature-Dependent Properties.

The temperature-dependent material properties that significantly affect the accuracy of the predictive models are density, thermal conductivity, specific heat capacity, and emissivity. Complete and well-documented sets of measurements of temperature-dependent material properties are available for some metals. However, to the best of our knowledge, similar standard documents for metallic alloys in a wide range of temperatures are unavailable. The standard method for implementing temperature-dependent properties is to linearly interpolate between the measured values provided that the measured values can be approximated linearly [149]. Moreover, due to the complexity of heat transfer mechanisms in an L-PBF process, precise determination of temperature-dependent properties above melting temperature is more difficult [150].

4.5.1 Thermal Conductivity.—Thermal conductivity is a quantity that determines the rate at which heat transfers through the material due to a temperature gradient. Thermal conductivity of a powder bed is smaller than the solid material due to higher porosity as the contact area between adjacent particles is small. Thermal conductivity is influenced by

NIST Author Manuscript

NIST Author Manuscript

NIST Author Manuscript

several factors including particle size and shape, particle size distribution, particle morphology, inter-particle distance, and thermal conductivity of the solid material and surrounding gas [75,151–154]. The effective thermal conductivity of the powder bed is different in the powder, melting, and solidification phases of the process and depends on the solidus and liquidus temperatures of the material in the melting phase [88,134]. Based on the review of literature, the source of uncertainties in thermal conductivity can be categorized as uncertainties related to powder properties, material properties, surrounding gas properties, and temperature.

4.5.2 Density.—Due to high temperature variation during the L-PBF process, from room temperature through melting, density of a material changes with temperature. In most cases, the density of the final part is higher than the powder bed density [155]. Availability and uncertainty in measured density at high temperature lead L-PBF models to assume (a) constant density, (b) linear variation between measured values, (c) different density in powder, molten, and solid phases of materials, or (d) constant density in solid region but a quadratic function of temperature in the liquid region [75,134]. These different assumptions can have considerable influence on the accuracy of models.

4.5.3 Specific Heat Capacity.—Temperature-dependent specific heat capacity follows a nonlinear function of temperature around the melting temperature in the melting phase to account for the latent heat of fusion [134,156]. However, to simplify the complexity of the model, some studies assumed a linear function of temperature in the solid region and a constant value of specific heat capacity in the liquid region [75]. Such simplification, in the absence of measured data, influences model accuracy.

4.5.4 Emissivity.—Emissivity is the property of a material that quantifies the efficiency of a surface to emit energy in the form of thermal radiation. It is defined as the ratio of the energy intensity radiated by the surface of a material to that radiated by a blackbody at the same temperature, wavelength, and viewing angle [157]. Emissivity is critical for the accurate prediction of the temperature of the molten pool and melt pool dimensions and can be used to calibrate thermal camera readings for temperature measurement. Emissivity of a material strongly depends on temperature and highly varies at elevated temperatures [158,159]. Powder bed emissivity also depends on factors such as wavelength, oxidation, contamination, surface texture, surface morphology, surface roughness [157–161], solid material emissivity, and powder bed porosity [162]. Furthermore, it is likely to have different values in the powder, melting, and solidified phases in the L-PBF process [127,163].

Based on the review of literature, the sources of uncertainty in powder bed emissivity can be categorized as uncertainties related to powder properties, material properties, in-bed porosity, and temperature. Uncertainty sources for powder bed absorptivity, powder bed thermal conductivity, and powder bed emissivity are compared in a fishbone diagram highlighting the common and different sources in Fig. 6.

Several other parameters that are of interest in L-PBF are preheat temperature, melting temperature, and latent heat of fusion. Uncertainties in these parameters also impact model accuracy.

NIST Author Manuscript

NIST Author Manuscript

NIST Author Manuscript

5 Challenges in Uncertainty Quantification for L-PBF

As can be seen from the review of model inaccuracies and parameter uncertainty sources presented in Secs. 3 and 4, the UQ in the L-PBF process is a difficult and tedious process. The modeling uncertainty of output quantity of interest is impacted by not only the parameter uncertainties but also the numerical and measurement uncertainties and cascading effect of one model output into other models. This cascading effect based on the summary of the review presented above is also depicted in Fig. 7.

To quantify the parameter uncertainty, a design of experiments approach needs to be planned. Such an approach would require consideration of simulation times of each model, model fidelity, model assumptions, uncertainty of input parameters, and the cascading effect shown in Fig. 7. Due to the large number of input parameters in L-PBF, a design of experiments approach can be challenging in terms of number of simulations and time required. Nevertheless, the uncertainty of an output quantity of interest will be a function of the uncertainties of input parameters (U_i), powder bed model (U_{PB}), heat source model (U_{HS}), melt pool model (U_{MP}), solidification model (U_S), and the residual stress model (U_{RS}), as shown in Eq. (1).

$$U_o = f\left(U_i,\ U_{PB},\ U_{HS},\ U_{MP},\ U_S,\ U_{RS}\right) \quad (1)$$

To quantify modeling uncertainty, simulation results S of the predictive model need to be validated against the experimental data D. The ASME V&V-20 standard [29], which discusses the sources of uncertainty and UQ methods in heat transfer and fluid mechanics models, can be suitable for L-PBF models as it involves thermally activated consolidation processes [87]. The interval within which modeling error falls is characterized by

$$\delta_{model}\,\epsilon\left[E \pm u_{val}\right] \quad (2)$$

where $\boldsymbol{E}$ is the comparison error between simulation result $\boldsymbol{S}$ and measurement data $\boldsymbol{D}$ and u_{val} is validation uncertainty, also known as modeling uncertainty, which accounts for all sources of uncertainty. Assuming that they are independent, it can be computed as follows

$$u_{val} = \sqrt{u_{num}^2 + u_{input}^2 + u_D^2} \quad (3)$$

where u_{num}, u_{input}, and u_D are numerical uncertainty, parameter uncertainty, and measurement uncertainty, respectively. Numerical uncertainty can be quantified using a grid convergence index [164], whereas measurement uncertainty is quantified as per the Guide to the expression of Uncertainty in Measurement (GUM) that standardized the evaluation and expression of uncertainty in measurement [165].

NIST Author Manuscript

NIST Author Manuscript

NIST Author Manuscript

Another aspect critical to uncertainty and inaccuracy of models is calibration uncertainty. As indicated earlier, models are calibrated to experimental measurements based on certain parameters. Depending on the physics considered in the model and input parameter ranges for the experiment, calibration will have associated uncertainty. Such uncertainty can play a wider role when comparing similar models to new experimental results. This effect is widely seen in recently concluded AMBench Tests [166].

The main goal of UQ studies in this work is to compare models having different fidelities and to identify (a) the parameter range over which low- and high-fidelity models can perform, (b) the ability to use data-driven models in combination with high-fidelity model results for specific parameter values, and (c) the speed at which these computations can be made using data-driven, physics-based, or hybrid models to quite in-process qualification for L-PBF. Recently, there are some research efforts on verification and validation and UQ of data-driven models for the prediction of melt pool dimensions and material property in metal L-PBF process [167,168]. Moreover, UQ framework based on data-driven surrogate models such as generalized polynomial chaos expansions [169] and Gaussian process [170,171] for quantifying sources of uncertainty in high-fidelity computational models have been the center of recent research interest in AM community.

Although many individual models describing the physics at different fidelity levels exist, there is still a lack of simulation models that include all the physics discussed in metal L-PBF process. The main hinderances for developing such a combined model are (a) speed and memory required to run individual models and (b) uncertainty and inaccuracy of the models. Even with modern Graphics Processing Unit (GPU), a high-fidelity model for even a single track runs several hours. For a realistic part, entire simulation may take anywhere from weeks to a month. For these reasons, many researchers are pursuing low-fidelity models, surrogate models, or data-driven models. These models have yet to prove their capability in comparison to high-fidelity physics-based models. As discussed throughout this paper, uncertainty and inaccuracy reporting with a model are needed to understand the advantages of one model over another. Very few studies focus on quantifying uncertainty and inaccuracy of individual models while none consider combined uncertainty of all the models. These are critical gaps in increasing the reliability of physics-based models for metal L-PBF simulations.

For complete part simulations, all five classes of simulation models have to consider geometry-related artifacts such as support structures, overhangs, thin walls, and bridges. Different physical phenomena exist for polymer PBF models, EBM models, and direct energy deposition type models. Although these phenomena are different, the modeling inaccuracies, calibration uncertainty, parameter uncertainty, and measurement uncertainty play similar role in model predictions.

Calibration uncertainty is another important aspect to be considered for simulation models. As detailed physics-based models are developed for metal L-PBF, multiple unmeasurable parameters emerge that need to be estimated and then calibrated for appropriate predictions from the models. Novel techniques to measure these parameters might need to be developed to reduce the calibration uncertainty.

NIST Author Manuscript

NIST Author Manuscript

NIST Author Manuscript

6 Conclusions

The paper comprehensively reviewed the five different phenomena (powder bed formation, heat absorption, melt pool formation, solidification, and residual stress) existing in L-PBF process, their simulation models, and associated uncertainties. The simulation models were reviewed focusing on the modeling assumptions. These assumptions in the models affect accuracy of the predictive model and related uncertainties. The sources of uncertainty of the critical input parameters (layer thickness, laser power, laser scan speed, absorptivity, thermal conductivity, density, specific heat capacity, and emissivity) were identified, and the uncertainty sources were mapped out in the fishbone diagram, giving first such detailed uncertainty map for L-PBF models.

The overall goal was to identify the sources of uncertainties and support the development of uncertainty quantification approach in simulation models of L-PBF for a given quantity of interest. With the complete review of model assumptions and parameter uncertainty sources, the development of UQ approach for L-PBF will be expedited. Furthermore, the cascading L-PBF model dependency and flow of model and parameter uncertainty will aid in reducing the effort in UQ. The UQ approach pursued in future will rely on design of experiments to showcase the impact of model/parameter sensitivities to the output quantity of interest. The ASME V&V 50 (Verification and Validation) Committee is developing a process to quantify uncertainty in a data-driven and hybrid physics-based model for advanced manufacturing including additive manufacturing [172]. Such a process, when developed, will further reduce the time and effort in conducting factorial design of experiments for such complex model interactions in L-PBF.

Acknowledgment

The authors gratefully acknowledge Jason Fox and Brandon Lane from the Engineering Laboratory at National Institute of Standards and Technology (NIST) for valuable discussions on the sources of model inaccuracy and parameter uncertainty.

References

[1]. Bourell DL, Beaman JJ, Marcus HL, and Barlow JW, 1990, “Solid Freeform Fabrication: An Advanced Manufacturing Approach,” International Solid Freeform Fabrication Symposium, University of Texas at Austin, Austin, TX, pp. 1–7.

[2]. Partee B, Hollister SJ, and Das S, 2006, “Selective Laser Sintering Process Optimization for Layered Manufacturing of CAPA 6501 Polycaprolactone Bone Tissue Engineering Scaffolds,” J. Manuf. Sci. Eng, 128(2), pp. 531–540.

[3]. Heinl P, Müller L, Körner C, Singer RF, and Müller FA, 2008, “Cellular Ti-6Al-4 V Structures With Interconnected Macro Porosity for Bone Implants Fabricated by Selective Electron Beam Melting,” Acta Biomater, 4(5), pp. 1536–1544. [PubMed: 18467197]

[4]. Yan C, Hao L, Hussein A, and Raymont D, 2012, “Evaluations of Cellular Lattice Structures Manufactured Using Selective Laser Melting,” Int. J. Mach. Tools Manuf, 62, pp. 32–38.

[5]. Petrovic V, Vicente Haro Gonzalez J, Jordá Ferrando O, Delgado Gordillo J, Ramón Blasco Puchades J, and Portolés Griñan L, 2011, “Additive Layered Manufacturing: Sectors of Industrial Application Shown Through Case Studies,” Int. J. Prod. Res, 49(4), pp. 1061–1079.

[6]. Kianian B, 2016, “Wohlers Report 2016: 3D Printing and Additive Manufacturing State of the Industry,” Annual Worldwide Progress Report, Wohlers Associates, Inc, Fort Collins, CO, pp. 355.

NIST Author Manuscript NIST Author Manuscript NIST Author Manuscript

[7]. Coykendall J, Cotteleer M, Holdowsky L, and Mahto M, 2014, 3D Opportunity in Aerospace and Defense, Deloitte University Press, pp. 1–28.

[8]. Chua CK, Leong KF, and Lim CS, 2010, Rapid Prototyping : Principles and Applications, World Scientific Publishing Co. PTE. Ltd, Singapore.

[9]. Holshouser C, Newell C, Palas S, Martin L, Duty C, Love L, Kunc V, Lind R, Lloyd P, Rowe J, Dehoff R, Peter W, and Blue C, 2013, "Out of Bounds Additive Manufacturing," Adv. Mater. Process, 171(3), pp. 15–17.

[10]. Herderick E, 2011, "Additive Manufacturing of Metals: A Review," Materials Science and Technology Conference and Exhibition 2011, MS and T'11, Vol. 2, pp. 1413–1425.

[11]. Gokuldoss PK, Kolla S, and Eckert J, 2017, "Additive Manufacturing Processes: Selective Laser Melting, Electron Beam Melting and Binder Jetting-Selection Guidelines," Materials (Basel), 10(6), 672.

[12]. Bourell DL, Leu MC, and Rosen DW, 2009, "Roadmap for Additive Manufacturing: Identifying the Future of Freeform Processing," Rapid Prototyp. J, 5(4), pp. 169–178.

[13]. Bauereiß A, Scharowsky T, and Körner C, 2014, "Defect Generation and Propagation Mechanism During Additive Manufacturing by Selective Beam Melting," J. Mater. Process. Technol, 214(11), pp. 2497–2504.

[14]. Kobryn PA, Ontko NR, Perkins LP, and Tiley JS, 2006, "Additive Manufacturing of Aerospace Alloys for Aircraft Structures," Meeting Proceedings RTO-MP-AVT-139, Paper 3, Neuilly-sur-Seine, France, 139(2006), pp. 1–14.

[15]. Schoinochoritis B, Chantzis D, and Salonitis K, 2014, "Simulation of Metallic Powder Bed Additive Manufacturing Processes With the Finite Element Method: A Critical Review," Proc. Inst. Mech. Eng. Part B J. Eng. Manuf, 231(1), pp. 96–117.

[16]. King WE, Anderson AT, Ferencz RM, Hodge NE, Kamath C, Khairallah SA, and Rubenchik AM, 2015, "Laser Powder Bed Fusion Additive Manufacturing of Metals; Physics, Computational, and Materials Challenges," Appl. Phys. Rev, 2(4), 041304.

[17]. Zhang Y, Lee WH, Wu L, Meng L, Jung Y-G, and Zhang J, 2018, Multiscale Multiphysics Modeling of Laser Powder Bed Fusion Process, Additive Manufacturing, Butterworth, Heinemann.

[18]. Zhang J, Zhang Y, Lee WH, Wu L, Choi HH, and Jung YG, 2018, "A Multi-Scale Multi-Physics Modeling Framework of Laser Powder Bed Fusion Additive Manufacturing Process," Met. Powder Rep, 73(3), pp. 151–157.

[19]. DebRoy T, Wei HL, Zuback JS, Mukherjee T, Elmer JW, Milewski JO, Beese AM, Wilson-Heid A, De A, and Zhang W, 2018, "Additive Manufacturing of Metallic Components—Process, Structure and Properties," Prog. Mater. Sci, 92, pp. 112–224.

[20]. Klassen A, Scharowsky T, and Körner C, 2014, "Evaporation Model for Beam Based Additive Manufacturing Using Free Surface Lattice Boltzmann Methods," J. Phys. D. Appl. Phys, 47(27), 275303.

[21]. Assouroko I, Lopez F, and Witherell P, 2016, "A Method for Characterizing Model Fidelity in Laser Powder Bed Fusion Additive Manufacturing," ASME 2016 International Mechanical Engineering Congress and Exposition, Phoenix, AZ, 11 11–17, pp. 1–13.

[22]. Roh B, Kumara SRT, Simpson TW, and Witherell P, 2016, "Ontology-Based Laser and Thermal Metamodels for Metal-Based Additive Manufacturing," ASME 2016 International Design Engineering Technical Conferences and Computers and Information in Engineering Conference, Charlotte, North Carolina, Aug. 21–24, pp. 1–8.

[23]. Witherell P, Feng S, Simpson TW, Saint John DB, Michaleris P, Liu Z-K, Chen L-Q, and Martukanitz R, 2014, "Toward Metamodels for Composable and Reusable Additive Manufacturing Process Models," J. Manuf. Sci. Eng, 136(6), 061025.

[24]. Hu Z, and Mahadevan S, 2017, "Uncertainty Quantification and Management in Additive Manufacturing: Current Status, Needs, and Opportunities," Int. J. Adv. Manuf. Technol, 93, pp. 2855–2874.

[25]. Lopez F, Witherell P, and Lane B, 2016, "Identifying Uncertainty in Laser Powder Bed Fusion Additive Manufacturing Models," ASME 2016 International Manufacturing Science and Engineering (MSEC2016), Blacksburg, VA, 6 27–7 1, Vol. 138, pp. 1–10.

NIST Author Manuscript NIST Author Manuscript NIST Author Manuscript

[26]. Tesfaye M, Yan W, Lin S, Ameta G, Fox J, and Witherell P (2018). “Quantifying Uncertainty In Laser Powder Bed Fusion Additive Manufacturing Models and Simulations,” Proceedings of the 29th Annual International Solid Freeform Fabrication Symposium, Austin, TX, 8 13–15.

[27]. Karayagiz K, Elwany A, Tapia G, Franco B, Johnson L, Ma J, Karaman I, and Arroyave R, 2018, “Numerical and Experimental Analysis of Heat Distribution in the Laser Powder Bed Fusion of Ti-6 Al-4 V,” IISE Trans, 5854, pp. 1–44.

[28]. Mahmoudi M, Tapia G, Karayagiz K, Franco B, Ma J, Arroyave R, Karaman I, and Elwany A, 2018, “Multivariate Calibration and Experimental Validation of a 3D Finite Element Thermal Model for Laser Powder-Bed Fusion Metal Additive Manufacturing,” Integr. Mater. Manuf. Innov, 7, 116.

[29]. ASME-V&V-20–2009, 2009, An Overview of ASME V&V 20: Standard for Verification and Validation in Computational Fluid Dynamics and Heat Transfer, American Society of Mechanical Engineers, New York.

[30]. Mindt HW, Megahed M, Lavery NP, Holmes MA, and Brown SGR, 2016, “Powder Bed Layer Characteristics: The Overseen First-Order Process Input,” Metall. Mater. Trans. A Phys. Metall. Mater. Sci, 47(8), pp. 3811–3822.

[31]. Parteli EJR, and Pöschel T, 2016, “Particle-Based Simulation of Powder Application in Additive Manufacturing,” Powder Technol, 288, pp. 96–102.

[32]. Dou X, Mao Y, and Zhang Y, 2014, “Effects of Contact Force Model and Size Distribution on Microsized Granular Packing,” J. Manuf. Sci. Eng, 136(2), 021003.

[33]. Xiang Z, Yin M, Deng Z, Mei X, and Yin G, 2016, “Simulation of Forming Process of Powder Bed for Additive Manufacturing,” J. Manuf. Sci. Eng, 138(8), 081002.

[34]. Parteli EJR, 2013, “DEM Simulation of Particles of Complex Shapes Using the Multisphere Method: Application for Additive Manufacturing,” AIP Conf. Proc, 1542(2013), pp. 185–188.

[35]. Herbold EB, Walton O, and Homel MA (2015). “Simulation of Powder Layer Deposition in Additive Manufacturing Processes Using the Discrete Element Method,” Report No. LLNL-TR-678550.

[36]. Jia T, Zhang Y, and Chen JK, 2011, “Dynamic Simulation of Particle Packing With Different Size Distributions,” J. Manuf. Sci. Eng, 133(2), 021011.

[37]. Körner C, Bauereiß A, and Attar E, 2013, “Fundamental Consolidation Mechanisms During Selective Beam Melting of Powders,” Model. Simul. Mater. Sci. Eng, 21(8), 085011.

[38]. Meakin P, and Jullien R, 1987, “Restructuring Effects in the Rain Model for Random Deposition,” J. Phys, 48(10), pp. 1651–1662.

[39]. Zhou J, Zhang Y, and Chen JK, 2009, “Numerical Simulation of Random Packing of Spherical Particles for Powder-Based Additive Manufacturing,” J. Manuf. Sci. Eng, 131(3), 031004.

[40]. Shi Y, and Zhang Y, 2008, “Simulation of Random Packing of Spherical Particles With Different Size Distributions,” Appl. Phys. A, 92(3), pp. 621–626.

[41]. Boley CD, Khairallah SA, and Rubenchik AM, 2015, “Calculation of Laser Absorption by Metal Powders in Additive Manufacturing,” Appl. Opt, 54(9), pp. 2477–82. [PubMed: 25968537]

[42]. Zhou J, Zhang Y, and Chen JK, 2009, “Numerical Simulation of Laser Irradiation to a Randomly Packed Bimodal Powder Bed,” Int. J. Heat Mass Transf, 52(13–14), pp. 3137–3146.

[43]. Tang HP, Qian M, Liu N, Zhang XZ, Yang GY, and Wang J, 2015, “Effect of Powder Reuse Times on Additive Manufacturing of Ti-6Al-4 V by Selective Electron Beam Melting,” JOM, 67(3), pp. 555–563.

[44]. Yap CY, Chua CK, Dong ZL, Liu ZH, Zhang DQ, Loh LE, and Sing SL, 2015, “Review of Selective Laser Melting: Materials and Applications,” Appl. Phys. Rev, 2(4), 041101.

[45]. Devesse W, De Baere D, and Guillaume P, 2014, “The Isotherm Migration Method in Spherical Coordinates With a Moving Heat Source,” Int. J. Heat Mass Transf, 75, pp. 726–735.

[46]. Rosenthal D, 1946, The Theory of Moving Sources of Heat and Its Application to Metal Treatments, ASME, Cambridge, pp. 849–866.

[47]. Malmelöv A, 2016, Modeling of Additive Manufacturing With Reduced Computational Effort; Simulation of Laser Metal Deposition with Inconel 625, Luleå University of Technology, Luleå, Sweden.

NIST Author Manuscript NIST Author Manuscript NIST Author Manuscript

[48]. Lindgren LE, Lundbäck A, Fisk M, Pederson R, and Andersson J, 2016, “Simulation of Additive Manufacturing Using Coupled Constitutive and Microstructure Models,” Addit. Manuf, 12, pp. 144–158.

[49]. Michaleris P, 2014, “Modeling Metal Deposition in Heat Transfer Analyses of Additive Manufacturing Processes,” Finite Elem. Anal. Des, 86, pp. 51–60.

[50]. Hussein A, Hao L, Yan C, and Everson R, 2013, “Finite Element Simulation of the Temperature and Stress Fields in Single Layers Built Without-Support in Selective Laser Melting,” Mater. Des, 52, pp. 638–647.

[51]. Gusarov AV, and Kruth JP, 2005, “Modelling of Radiation Transfer in Metallic Powders at Laser Treatment,” Int. J. Heat Mass Transf, 48(16), pp. 3423–3434.

[52]. Meier C, Penny RW, Zou Y, Gibbs JS, and Hart AJ, 2017, “Thermophysical Phenomena in Metal Additive Manufacturing by Selective Laser Melting: Fundamentals, Modeling, Simulation and Experimentation,” Annu. Rev. Heat Transf, abs/1709.09510.

[53]. Li JF, Li L, and Stott FH, 2004, “Comparison of Volumetric and Surface Heating Sources in the Modeling of Laser Melting of Ceramic Materials,” Int. J. Heat Mass Transf, 47(6–7), pp. 1159–1174.

[54]. Fischer P, Romano V, Weber HP, Karapatis NP, Boillat E, and Glardon R, 2003, “Sintering of Commercially Pure Titanium Powder With a Nd:YAG Laser Source,” Acta Mater, 51(6), pp. 1651–1662.

[55]. Chen Q, Guillemot G, Gandin C-A, and Bellet M, 2017, “Three-Dimensional Finite Element Thermomechanical Modeling of Additive Manufacturing by Selective Laser Melting for Ceramic Materials,” Addit. Manuf, 16, pp. 124–137.

[56]. Körner C, Attar E, and Heinl P, 2011, “Mesoscopic Simulation of Selective Beam Melting Processes,” J. Mater. Process. Technol, 211(6), pp. 978–987.

[57]. Masoomi M, Thompson SM, and Shamsaei N, 2017, “Laser Powder Bed Fusion of Ti-6Al-4 V Parts: Thermal Modeling and Mechanical Implications,” Int. J. Mach. Tools Manuf, 118–119, pp. 73–90.

[58]. Yan W, Smith J, Ge W, Lin F, and Liu WK, 2015, “Multiscale Modeling of Electron Beam and Substrate Interaction: A New Heat Source Model,” Comput. Mech, 56(2), pp. 265–276.

[59]. Wang X, and Kruth J, 2000, “Energy Absorption and Penetration in Selective Laser Sintering: A Ray Tracing Model,” Proceedings of the International Conference on Mathematical Modelling and Simulation of Metal Technologies, pp. 673–683.

[60]. Markl M, and Korner C, 2016, “Multiscale Modeling of Powder Bed–Based Additive Manufacturing,” Annu. Rev. Mater. Res, 46, pp. 1–34.

[61]. Mukherjee T, Wei HL, De A, and DebRoy T, 2018, “Heat and Fluid Flow in Additive Manufacturing—Part I: Modeling of Powder Bed Fusion,” Comput. Mater. Sci, 150, pp. 304–313.

[62]. Criales LE, Arısoy YM, Lane B, Moylan S, Donmez A, and Özel T, 2017, “Predictive Modeling and Optimization of Multi-Track Processing for Laser Powder Bed Fusion of Nickel Alloy 625,” Addit. Manuf, 13, pp. 14–36.

[63]. Dai D, and Gu D, 2015, “Tailoring Surface Quality Through Mass and Momentum Transfer Modeling Using a Volume of Fluid Method in Selective Laser Melting of TiC/AlSi10Mg Powder,” Int. J. Mach. Tools Manuf, 88, pp. 95–107.

[64]. Khairallah SA, Anderson AT, Rubenchik A, and King WE, 2016, “Laser Powder-Bed Fusion Additive Manufacturing: Physics of Complex Melt Flow and Formation Mechanisms of Pores, Spatter, and Denudation Zones,” Acta Mater, 108, pp. 36–45.

[65]. Khairallah SA, and Anderson A, 2014, “Mesoscopic Simulation Model of Selective Laser Melting of Stainless Steel Powder,” J. Mater. Process. Technol, 214(11), pp. 2627–2636.

[66]. Das S, 2003, “Physical Aspects of Process Control in Selective Laser Sintering of Metals,” Adv. Eng. Mater, 5(10), pp. 701–711.

[67]. Gusarov AV, Yadroitsev I, Bertrand P, and Smurov I, 2007, “Heat Transfer Modelling and Stability Analysis of Selective Laser Melting,” Appl. Surf. Sci, 254, pp. 975–979.

NIST Author Manuscript NIST Author Manuscript NIST Author Manuscript

[68]. Juechter V, Scharowsky T, Singer RF, and Körner C, 2014, “Processing Window and Evaporation Phenomena for Ti-6Al-4 V Produced by Selective Electron Beam Melting,” Acta Mater, 76, pp. 252–258.

[69]. Sun X, Zhou W, Kikuchi K, Nomura N, Kawasaki A, Doi H, Tsutsumi Y, and Hanawa T, 2017, “Fabrication and Characterization of a Low Magnetic Zr-1Mo Alloy by Powder Bed Fusion Using a Fiber Laser,” Metals (Basel), 7(11), p. 501.

[70]. Liu YJ, Li SJ, Wang HL, Hou WT, Hao YL, Yang R, Sercombe TB, and Zhang LC, 2016, “Microstructure, Defects and Mechanical Behavior of Beta-Type Titanium Porous Structures Manufactured by Electron Beam Melting and Selective Laser Melting,” Acta Mater, 113, pp. 56–67.

[71]. Verhaeghe F, Craeghs T, Heulens J, and Pandelaers L, 2009, “A Pragmatic Model for Selective Laser Melting with Evaporation,” Acta Mater, 57(20), pp. 6006–6012.

[72]. Lee Y, 2015, Simulation of Laser Additive Manufacturing and Its Applications, The Ohio State University, Columbus, OH.

[73]. Zeng K, Pal D, and Stucker BE, 2012, “A Review of Thermal Analysis Methods in Laser Sintering and Selective Laser Melting,” Proceedings of Solid Freeform Fabrication Symposium, University of Texas at Austin, Austin, pp. 796–814.

[74]. Roberts IA, Wang CJ, Esterlein R, Stanford M, and Mynors DJ, 2009, “A Three-Dimensional Finite Element Analysis of the Temperature Field During Laser Melting of Metal Powders in Additive Layer Manufacturing,” Int. J. Mach. Tools Manuf, 49(12–13), pp. 916–923.

[75]. Antony K, Arivazhagan N, and Senthilkumaran K, 2014, “Numerical and Experimental Investigations on Laser Melting of Stainless Steel 316L Metal Powders,” J. Manuf. Process, 16(3), pp. 345–355.

[76]. Hodge NE, Ferencz RM, and Solberg JM, 2014, “Implementation of a Thermomechanical Model for the Simulation of Selective Laser Melting,” Comput. Mech, 54(1), pp. 33–51.

[77]. Zhang Y, Guillemot G, Bernacki M, and Bellet M, 2018, “Macroscopic Thermal Finite Element Modeling of Additive Metal Manufacturing by Selective Laser Melting Process,” Comput. Methods Appl. Mech. Eng, 331, pp. 514–535.

[78]. Zhou W, Loney D, Fedorov AG, Degertekin FL, and Rosen DW, 2013, “Lattice Boltzmann Simulations of Multiple Droplet Interactions During Impingement on the Substrate,” International Solid Freeform Fabrication Symposium—An Additive Manufacturing Conference, pp. 606–621.

[79]. Lee YS, and Zhang W, 2015, “Mesoscopic Simulation of Heat Transfer and Fluid Flow in Laser Powder Bed Additive Manufacturing,” International Solid Freeform Fabrication Symposium—An Additive Manufacturing Conference, pp. 1154–1165.

[80]. Yan W, Ge W, Qian Y, Lin S, Zhou B, Liu WK, Lin F, and Wagner GJ, 2017, “Multi-Physics Modeling of Single/Multiple-Track Defect Mechanisms in Electron Beam Selective Melting,” Acta Mater, 134, pp. 324–333.

[81]. Qiu C, Panwisawas C, Ward M, Basoalto HC, Brooks JW, and Attallah MM, 2015, “On the Role of Melt Flow Into the Surface Structure and Porosity Development During Selective Laser Melting,” Acta Mater, 96, pp. 72–79.

[82]. Gürtler FJ, Karg M, Leitz KH, and Schmidt M, 2013, “Simulation of Laser Beam Melting of Steel Powders Using the Three-Dimensional Volume of Fluid Method,” Phys. Procedia, 41, pp. 881–886.

[83]. Megahed M, Mindt H-W, N’Dri N, Duan H, and Desmaison O, 2016, “Metal Additive-Manufacturing Process and Residual Stress Modeling,” Integr. Mater. Manuf. Innov, 5(1), pp. 4.

[84]. Tang C, Tan JL, and Wong CH, 2018, “A Numerical Investigation on the Physical Mechanisms of Single Track Defects in Selective Laser Melting,” Int. J. Heat Mass Transf, 126, pp. 957–968.

[85]. Masoomi M, Pegues JW, Thompson SM, and Shamsaei N, 2018, “A Numerical and Experimental Investigation of Convective Heat Transfer During Laser-Powder Bed Fusion,” Addit. Manuf, 22, pp. 729–745.

[86]. King W, Anderson AT, Ferencz RM, Hodge NE, Kamath C, and Khairallah SA, 2015, “Overview of Modelling and Simulation of Metal Powder Bed Fusion Process at Lawrence Livermore National Laboratory,” Mater. Sci. Technol, 31(8), pp. 957–968.

NIST Author Manuscript NIST Author Manuscript NIST Author Manuscript

[87]. Lopez F, Witherell P, and Lane B, 2016, "Identifying Uncertainty in Laser Powder Bed Fusion Additive Manufacturing Models," J. Mech. Des, 138, pp. 1–4.

[88]. Ma L, Fong J, Lane B, Moylan S, Filliben J, Heckert A, and Levine L, 2015, "Using Design of Experiments in Finite Element Modeling to Identify Critical Variables for Laser Powder Bed Fusion," 2015 Annual International Solid Freeform Fabrication Symposium—An Additive Manufacturing Conference, Austin, TX, Aug. 10–12, pp. 219–228.

[89]. Foroozmehr A, Badrossamay M, Foroozmehr E, and Golabi S, 2016, "Finite Element Simulation of Selective Laser Melting Process Considering Optical Penetration Depth of Laser in Powder Bed," Mater. Des, 89, pp. 255–263.

[90]. Song B, Dong S, Liao H, and Coddet C, 2012, "Process Parameter Selection for Selective Laser Melting of Ti6Al4 V Based on Temperature Distribution Simulation and Experimental Sintering," Int. J. Adv. Manuf. Technol, 61(9–12), pp. 967–974.

[91]. Cheng B, and Chou K, 2015, "Melt Pool Evolution Study in Selective Laser Melting," 26th Annual International Solid Freeform Fabrication Symposium—An Additive Manufacturing Conference, Austin, TX, 8 10–12, 53, pp. 1182–1194.

[92]. Foteinopoulos P, Papacharalampopoulos A, and Stavropoulos P, 2018, "On Thermal Modeling of Additive Manufacturing Processes," CIRP J. Manuf. Sci. Technol, 20, pp. 66–83.

[93]. Rausch AM, Küng VE, Pobel C, Markl M, and Körner C, 2017, "Predictive Simulation of Process Windows for Powder Bed Fusion Additive Manufacturing: Influence of the Powder Bulk Density," Materials (Basel), 10(10), 1117.

[94]. Wu YC, San CH, Chang CH, Lin HJ, Marwan R, Baba S, and Hwang WS, 2018, "Numerical Modeling of Melt-Pool Behavior in Selective Laser Melting With Random Powder Distribution and Experimental Validation," J. Mater. Process. Technol, 254, pp. 72–78.

[95]. Pei W, Zhengying W, Zhen C, Junfeng L, Shuzhe Z, and Jun D, 2017, "Numerical Simulation and Parametric Analysis of Selective Laser Melting Process of AlSi10Mg Powder," Appl. Phys. A, 123(8), pp. 540.

[96]. Panwisawas C, Qiu C, Anderson MJ, Sovani Y, Turner RP, Attallah MM, Brooks JW, and Basoalto HC, 2017, "Mesoscale Modelling of Selective Laser Melting: Thermal Fluid Dynamics and Microstructural Evolution," Comput. Mater. Sci, 126, pp. 479–490.

[97]. Heeling T, Cloots M, and Wegener K, 2017, "Melt Pool Simulation for the Evaluation of Process Parameters in Selective Laser Melting," Addit. Manuf, 14, pp. 116–125.

[98]. Glicksman ME, 2011, Principles of Solidification: An Introduction to Modern Casting and Crystal Growth Concepts, Springer Science + Business Media, Berlin/Heidelberg, Germany.

[99]. Gockel J, Beutha J, and Taminger K, 2014, "Integrated Control of Solidification Microstructure and Melt Pool Dimensions in Electron Beam Wire Feed Additive Manufacturing of Ti-6Al-4 V," Addit. Manuf, 4, pp. 119–126.

[100]. Hanzl P, Zetek M, Bakša T, and Kroupa T, 2015, "The Influence of Processing Parameters on the Mechanical Properties of SLM Parts," Procedia Eng, 100, pp. 1405–1413.

[101]. Zinoviev A, Zinovieva O, Ploshikhin V, Romanova V, and Balokhonov R, 2016, "Evolution of Grain Structure During Laser Additive Manufacturing. Simulation by a Cellular Automata Method," Mater. Des, 106, pp. 321–329.

[102]. Wu AS, Brown DW, Kumar M, Gallegos GF, and King WE, 2014, "An Experimental Investigation into Additive Manufacturing-Induced Residual Stresses in 316L Stainless Steel," Metall. Mater. Trans. A Phys. Metall. Mater. Sci, 45(13), pp. 6260–6270.

[103]. Arısoy YM, Criales LE, Özel T, Lane B, Moylan S, and Donmez A, 2017, "Influence of Scan Strategy and Process Parameters on Microstructure and Its Optimization in Additively Manufactured Nickel Alloy 625 via Laser Powder Bed Fusion," Int. J. Adv. Manuf. Technol, 90(5–8), pp. 1393–1417.

[104]. Boettinger WJ, Coriell SR, Greer AL, Karma A, Kurz W, Rappaz M, and Trivedi R, 2000, "Solidification Microstructures: Recent Developments, Future Directions," Acta Mater, 48(1), pp. 43–70.

[105]. Chen L-Q, 2002, "Phase-Field Models for Microstructure Evolution," Annu. Rev. Mater. Res, 32(1), pp. 113–140.

NIST Author Manuscript NIST Author Manuscript NIST Author Manuscript

[106]. Keller T, Lindwall G, Ghosh S, Ma L, Lane BM, Zhang F, Kattner UR, Lass EA, Heigel JC, Idell Y, Williams ME, Allen AJ, Guyer JE, and Levine LE, 2017, "Application of Finite Element, Phase-Field, and CALPHAD-Based Methods to Additive Manufacturing of Ni-Based Superalloys," Acta Mater, 139, pp. 244–253. [PubMed: 29230094]

[107]. Gong X, and Chou K, 2015, "Phase-Field Modeling of Microstructure Evolution in Electron Beam Additive Manufacturing," JOM, 67(5), pp. 1176–1182.

[108]. Zaeem MA, Yin H, and Felicelli SD, 2012, "Comparison of Cellular Automaton and Phase Field Models to Simulate Dendrite Growth in Hexagonal Crystals," J. Mater. Sci. Technol, 28(2), pp. 137–146.

[109]. Li X, and Tan W, 2017, "3-Dimensional Cellular Automata Simulation of Grain Structure in Metal Additive Manufacturing Processes," International Solid Freeform Fabrication Symposium —An Additive Manufacturing Conference, pp. 1030–1047.

[110]. Nath P, Hu Z, and Mahadevan S, 2017, "Multi-Level Uncertainty Quantification in Additive Manufacturing," Proceedings of the 28th Annual International Solid Freeform Fabrication Symposium – An Additive Manufacturing Conference, pp. 922–937.

[111]. Rai A, Markl M, and Körner C, 2016, "A Coupled Cellular Automaton – Lattice Boltzmann Model for Grain Structure Simulation During Additive Manufacturing," Comput. Mater. Sci, 124, pp. 37–48.

[112]. Lopez-Botello O, Martinez-Hernandez U, Ramírez J, Pinna C, and Mumtaz K, 2017, "Two-Dimensional Simulation of Grain Structure Growth Within Selective Laser Melted AA-2024," Mater. Des, 113, pp. 369–376.

[113]. Parry L, Ashcroft I, Bracket D, and Wildman RD, 2015, "Investigation of Residual Stresses in Selective Laser Melting," Key Eng. Mater, 627, pp. 129–132.

[114]. Jiang W, Dalgarno KW, and Childs THC, 2002, "Finite Element Analysis of Residual Stresses and Deformations in Direct Metal SLS Process," Proceedings of Solid Freeform Fabrication Symposium, pp. 340–348.

[115]. Hodge NE, Ferencz RM, and Vignes RM, 2016, "Experimental Comparison of Residual Stresses for a Thermomechanical Model for the Simulation of Selective Laser Melting," Addit. Manuf, 12, pp. 159–168.

[116]. Mercelis P, and Kruth J, 2006, "Residual Stresses in Selective Laser Sintering and Selective Laser Melting," Rapid Prototyp. J, 12(5), pp. 254–265.

[117]. Parry L, Ashcroft IA, and Wildman RD, 2016, "Understanding the Effect of Laser Scan Strategy on Residual Stress in Selective Laser Melting Through Thermo-Mechanical Simulation," Addit. Manuf, 12, pp. 1–15.

[118]. Lu Y, Wu S, Gan Y, Huang T, Yang C, Junjie L, and Lin J, 2015, "Study on the Microstructure, Mechanical Property and Residual Stress of SLM Inconel-718 Alloy Manufactured by Differing Island Scanning Strategy," Opt. Laser Technol, 75, pp. 197–206.

[119]. Ali H, Ma L, Ghadbeigi H, and Mumtaz K, 2017, "In-Situ Residual Stress Reduction, Martensitic Decomposition and Mechanical Properties Enhancement Through High Temperature Powder Bed Pre-Heating of Selective Laser Melted Ti6Al4 V," Mater. Sci. Eng. A, 695, pp. 211–220.

[120]. Shiomi M, Osakada K, Nakamura K, Yamashita T, and Abe F, 2004, "Residual Stress Within Metallic Model Made by Selective Laser Melting Process," CIRP Ann. Manuf. Technol, 53, pp. 195–198.

[121]. Zaeh MF, and Branner G, 2010, "Investigations on Residual Stresses and Deformations in Selective Laser Melting," Prod. Eng, 4(1), pp. 35–45.

[122]. Denlinger ER, Heigel JC, and Michaleris P, 2015, "Residual Stress and Distortion Modeling of Electron Beam Direct Manufacturing Ti-6Al-4 V," Proc. Inst. Mech. Eng. Part B J. Eng. Manuf, 229(10), pp. 1803–1813.

[123]. Li Y, Zhou K, Tan P, Tor SB, Chua CK, and Leong KF, 2018, "Modeling Temperature and Residual Stress Fields in Selective Laser Melting," Int. J. Mech. Sci, 136, pp. 24–35.

[124]. Yang YP, Jamshidinia M, Boulware P, and Kelly SM, 2018, "Prediction of Microstructure, Residual Stress, and Deformation in Laser Powder Bed Fusion Process," Comput. Mech, 61(5), pp. 599–615.

NIST Author Manuscript NIST Author Manuscript NIST Author Manuscript

[125]. Martukanitz R, Michaleris P, Palmer T, DebRoy T, Liu ZK, Otis R, Heo TW, and Chen LQ, 2014, “Toward an Integrated Computational System for Describing the Additive Manufacturing Process for Metallic Materials,” Addit. Manuf, 1, pp. 52–63.

[126]. Yadroitsev I, 2009, Selective Laser Melting : Direct Manufacturing of 3D-Objects by Selective Laser Melting of Metal Powders, LAP LAMBERT Academic Publishing, AG & Co KG: Saarbrücken, Germany.

[127]. Mahesh M, Lane B, Donmez A, Feng S, Moylan S, and Fesperman R, 2015, “Measurement Science Needs for Real-Time Control of Additive Manufacturing Powder Bed Fusion Processes,” Natl. Inst. Stand. Technol pp. 1–50.

[128]. Ma M, Wang Z, Gao M, and Zeng X, 2015, “Layer Thickness Dependence of Performance in High-Power Selective Laser Melting of 1Cr18Ni9Ti Stainless Steel,” J. Mater. Process. Technol, 215(1), pp. 142–150.

[129]. Zhang B, Dembinski L, and Coddet C, 2013, “The Study of the Laser Parameters and Environment Variables Effect on Mechanical Properties of High Compact Parts Elaborated by Selective Laser Melting 316L Powder,” Mater. Sci. Eng. A, 584, pp. 21–31.

[130]. Sufiiarov VS, Popovich AA, Borisov EV, Polozov IA, Masaylo DV, and Orlov AV, 2017, “The Effect of Layer Thickness at Selective Laser Melting,” Procedia Eng, 174, pp. 126–134.

[131]. Savalani MM, and Pizarro JM, 2016, “Effect of Preheat and Layer Thickness on Selective Laser Melting (SLM) of Magnesium,” Rapid Prototyp.J, 22(1), pp. 115–122.

[132]. Dingal S, Pradhan TR, Sundar JKS, Choudhury AR, and Roy SK, 2008, “The Application of Taguchi’s Method in the Experimental Investigation of the Laser Sintering Process,” Int. J. Adv. Manuf. Technol, 38(9–10), pp. 904–914.

[133]. McGlauflin M, and Moylan S, 2016, “Powder Bed Layer Geometry,” ASPE/euspen Summer Topical Meeting. Advancing Precision in Additive Manufacturing, Raleigh, NC, 6 27–30, pp. 108–113.

[134]. Riedlbauer D, Scharowsky T, Singer RF, Steinmann P, Körner C, and Mergheim J, 2017, “Macroscopic Simulation and Experimental Measurement of Melt Pool Characteristics in Selective Electron Beam Melting of Ti-6Al-4 V,” Int. J. Adv. Manuf. Technol, 88(5–8), pp. 1309–1317.

[135]. Bergman S, 2016, “Novel Beam Diagnostics Improve Laser Additive Manufacturing,” A Coherent Whitepaper.

[136]. King WE, Barth HD, Castillo VM, Gallegos GF, Gibbs JW, Hahn DE, Kamath C, and Rubenchik AM, 2014, “Observation of Keyhole-Mode Laser Melting in Laser Powder-Bed Fusion Additive Manufacturing,” J. Mater. Process. Technol, 214(12), pp. 2915–2925.

[137]. Weingarten KJ, Braun B, and Keller U, 1995, “In Situ Small-Signal Gain of Solid-State Lasers Determined From Relaxation Oscillation Frequency Measurements,” Opt. Lett, 19(15), pp. 1140–1142.

[138]. Schlatter A, Zeller SC, Grange R, Paschotta R, and Keller U, 2004, “Pulse-Energy Dynamics of Passively Mode-Locked Solid-State Lasers Above the Q-Switching Threshold,” J. Opt. Soc. Am. B, 21(8), pp. 1469–1478.

[139]. Kusuma C, 2016, The Effect of Laser Power and Scan Speed on Melt Pool Characteristics of Pure Titanium and Ti-6Al-4V Alloy for Selective Laser Melting, Wright State University, Dayton, OH.

[140]. Yeung H, Neira J, Lane B, Fox J, and Lopez F, 2016, “Laser Path Planning and Power Control Strategies for Powder,” Proceedings of the Solid Freeform Fabrication Symposium, Austin, TX, 8 8–10, pp. 113–127.

[141]. ASPE 2014 Spring Topical Meeting, 2014, Proceedings of Dimensional Accuracy and Surface Finish in Additive Manufacturing, University of California, CA.

[142]. Criales LE, Arısoy YM, and Özel T, 2016, “Sensitivity Analysis of Material and Process Parameters in Finite Element Modeling of Selective Laser Melting of Inconel 625,” Int. J. Adv. Manuf. Technol, 86(9–12), pp. 2653–2666.

[143]. Rubenchik A, Wu S, Mitchell S, Golosker I, LeBlanc M, and Peterson N, 2015, “Direct Measurements of Temperature-Dependent Laser Absorptivity of Metal Powders,” Appl. Opt, 54(24), pp. 7230. [PubMed: 26368757]

NIST Author Manuscript NIST Author Manuscript NIST Author Manuscript

[144]. Cho JH, and Na SJ, 2006, “Implementation of Real-Time Multiple Reflection and Fresnel Absorption of Laser Beam in Keyhole,”J. Phys. D. Appl. Phys, 39(24), pp. 5372–5378.

[145]. Trapp J, Rubenchik AM, Guss G, and Matthews MJ, 2017, “In Situ Absorptivity Measurements of Metallic Powders During Laser Powder-Bed Fusion Additive Manufacturing,” Appl. Mater. Today, 9, pp. 341–349.

[146]. Tolochko NK, Laoui T, Khlopkov YV, Mozzharov SE, Titov VI, and Ignatiev MB, 2000, “Absorptance of Powder Materials Suitable for Laser Sintering,” Rapid Prototyp. J, 6(3), pp. 155–160.

[147]. Kruth JP, Wang X, Laoui T, and Froyen L, 2003, “Assembly Automation Lasers and Materials in Selective Laser Sintering ‘Absorptance of Powder Materials Suitable for Laser Sintering’ Lasers and Materials in Selective Laser Sintering,” Assem. Autom, 2315(5), pp. 357–371.

[148]. Sainte-Catherine C, Jeandin M, Kechemair D, Ricaud J-P, and Sabatier L, 1991, “Study of Dynamic Absorptivity at 10.6 Mm (Co2) and 1.06 Mm (Nd-Yag) Wavelengths as a Function of Temperature,” J. Phys. IV, 1, pp. 1–8.

[149]. Gouge M, and Michaleris P, 2017, Thermo-Mechanical Modeling of Additive Manufacturing, Elsevier Science & Technology Books, New York.

[150]. Li D, Liu Y, Chen Y, Ren J, Liu J, and Yin J, 2011, Simulation of Transient Temperature Field in the Selective Laser Sintering Process of W/Ni Powder Mixture, International Federation for Information Processing, pp. 494–503.

[151]. Rombouts M, Froyen L, Gusarov AV, Bentefour EH, and Glorieux C, 2005, “Photopyroelectric Measurement of Thermal Conductivity of Metallic Powders,” J. Appl. Phys, 97(2), pp. 1–9.

[152]. Alkahari MR, Furumoto T, Ueda T, Hosokawa A, Tanaka R, and Abdul Aziz MS, 2012, “Thermal Conductivity of Metal Powder and Consolidated Material Fabricated via Selective Laser Melting,” Key Eng. Mater, 523–524, pp. 244–249.

[153]. Shapiro M, Dudko V, Royzen V, Krichevets Y, Lekhtmakher S, Grozubinsky V, Shapira M, and Brill M, 2004, “Characterization of Powder Beds by Thermal Conductivity: Effect of Gas Pressure on the Thermal Resistance of Particle Contact Points,” Part. Part. Syst. Charact, 21(4), pp. 268–275.

[154]. Childs THC, Hauser C, and Badrossamay M, 2005, “Selective Laser Sintering (Melting) of Stainless and Tool Steel Powders: Experiments and Modelling,” Proc. Inst. Mech. Eng. Part B J. Eng. Manuf, 219(4), pp. 339–357.

[155]. Kolossov S, Boillat E, Glardon R, Fischer P, and Locher M, 2004, “3D FE Simulation for Temperature Evolution in the Selective Laser Sintering Process,” Int. J. Mach. Tools Manuf, 44(2–3), pp. 117–123.

[156]. Zhang DQ, Cai QZ, Liu JH, Zhang L, and Li RD, 2010, “Select Laser Melting of W-Ni-Fe Powders: Simulation and Experimental Study,” Int. J. Adv. Manuf. Technol, 51(5–8), pp. 649–658.

[157]. Wen C, and Mudawar I, 2002, “Experimental Investigation of Emissivity of Aluminum Alloys and Temperature Determination Using,” J. Mater. Eng. Perform, 11, pp. 551–562.

[158]. Sih SS, and Barlow JW, 1995, “Emissivity of Powder Beds,” Sixth International Solid Freeform Fabrication Symposium, pp. 402–408.

[159]. Kieruj P, Przestacki D, and Chwalczuk T, 2016, “Determination of Emissivity Coefficient of Heat-Resistant Super Alloys and Cemented Carbide,” Arch. Mech. Technol. Mater, 36(1), pp. 30–34.

[160]. Delgado J, Ciurana J, and Rodríguez CA, 2012, “Influence of Process Parameters on Part Quality and Mechanical Properties for DMLS and SLM with Iron-Based Materials,” Int. J. Adv. Manuf. Technol, 60(5–8), pp. 601–610.

[161]. del Campo L, Pérez-Sáez RB, González-Fernández L, Esquisabel X, Fernández I, González-Martín P, and Tello MJ, 2010, “Emissivity Measurements on Aeronautical Alloys,” J. Alloys Compd, 489(2), pp. 482–487.

[162]. Sih SS, and Barlow JW, 2004, “The Prediction of the Emissivity and Thermal Conductivity of Powder Beds,” Part. Sci. Technol, 22(4), pp. 427–440.

[163]. Rodriguez E, Medina F, Espalin D, Terrazas C, Muse D, Henry C, MacDonald E, and Wicker RB, 2012, “Integration of a Thermal Imaging Feedback Control System in Electron Beam

NIST Author Manuscript

NIST Author Manuscript

NIST Author Manuscript

Melting," 23rd Annual International Solid Freeform Fabrication Symposium—An Additive Manufacturing Conference, pp. 945–961.

[164]. Roache P, "Code Verification by the Method of Manufactured Solutions,"J. Fluids Eng, 124(1), pp. 4–10.

[165]. J. C. F. G. I. M., 2008, "JCGM: Evaluation of Measurement Data—Guide to the Expression of Uncertainty in Measurement," Int. Organ. Stand. Geneva ISBN, 50, pp. 134.

[166]. AMBench, 2018, https://www.nist.gov/ambench, Accessed Oct. 18, 2018].

[167]. Kamath C, 2016, "Data Mining and Statistical Inference in Selective Laser Melting," Int. J. Adv. Manuf. Technol, 86(5–8), pp. 1659–1677.

[168]. Reed HM, Tomasetti T, Pires M, Vinci RP, Castro M, Robeck C, Tomasetti T, Dc W, Verdonik T, and Haden CV, 2017, "Statistically-Substantiated Density Characterizations of Additively Manufactured Steel Alloys Through Verification, Validation, and Uncertainty Quantification," IEEE International Conference on Big Data (Big Data), Boston, MA, pp. 1–9.

[169]. Tapia G, King WE, Arroyave R, Johnson L, Karaman I, and Elwany A, 2018, "Uncertainty Propagation Analysis of Computational Models in Laser Powder Bed Fusion Additive Manufacturing Using Polynomial Chaos Expansions," J. Manuf. Sci. Eng, 140, 121006.

[170]. Tapia G, Khairallah S, Matthews M, King WE, and Elwany A, 2017, "Gaussian Process-Based Surrogate Modeling Framework for Process Planning in Laser Powder-Bed Fusion Additive Manufacturing of 316L Stainless Steel," Int. J. Adv. Manuf. Technol, 94, pp. 1–13.

[171]. Li J, Jin R, and Yu HZ, 2018, "Integration of Physically-Based and Data-Driven Approaches for Thermal Field Prediction in Additive Manufacturing," Mater. Des, 139, pp. 473–485.

[172]. V&V 50 - Committee Page, https://cstools.asme.org/csconnect/committeePages.Cfm?Committee=101978604, Accessed October 18, 2018.

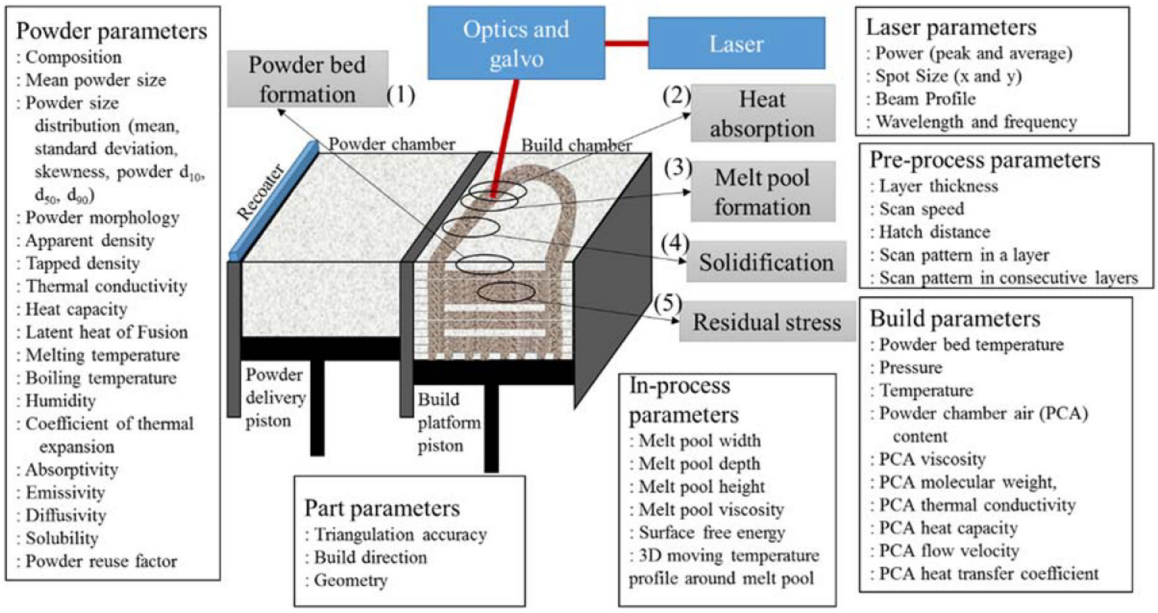

Fig. 1.
Overview of L-PBF process with different physical phenomena and process parameters

NIST Author Manuscript
NIST Author Manuscript
NIST Author Manuscript

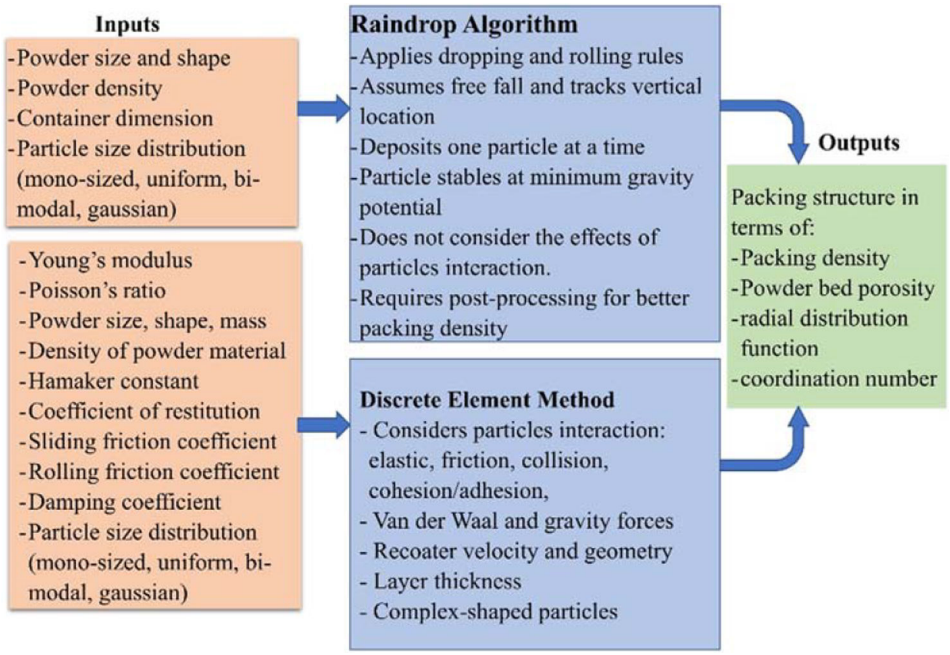

Fig. 2.

Input, output, and characteristics of powder bed models: raindrop algorithm [37–40] and discrete element method [32–36]

NIST Author Manuscript NIST Author Manuscript NIST Author Manuscript

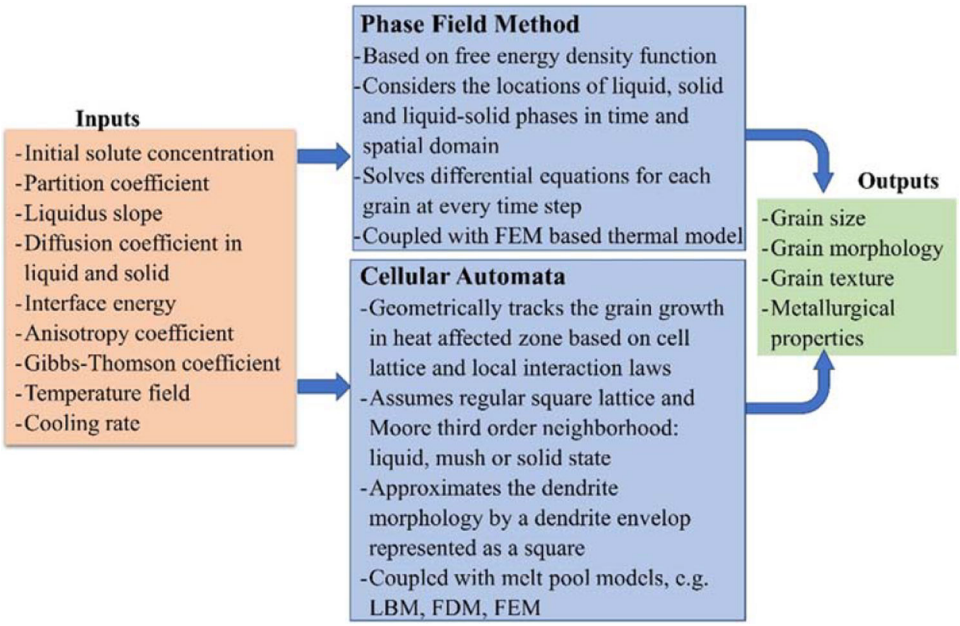

Fig. 3.

Inputs, outputs, and characteristics of solidification models: phase field method [105–108] and cellular automaton [101,108–111]

NIST Author Manuscript NIST Author Manuscript NIST Author Manuscript

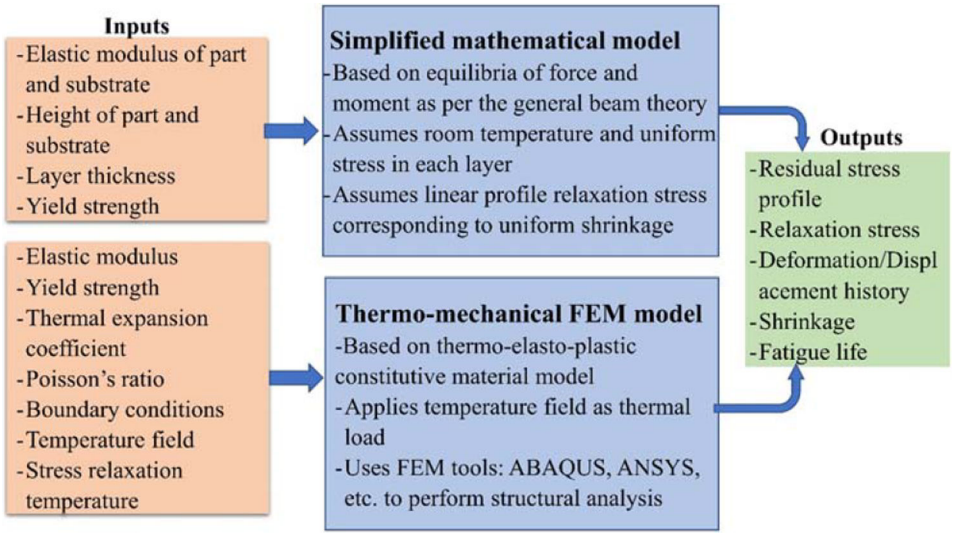

Fig. 4.

Inputs, outputs, and characteristics of residual stress models: simplified mathematical model [116] and thermomechanical FEM model [50,76,121–124]

NIST Author Manuscript NIST Author Manuscript NIST Author Manuscript

NIST Author Manuscript

NIST Author Manuscript

NIST Author Manuscript

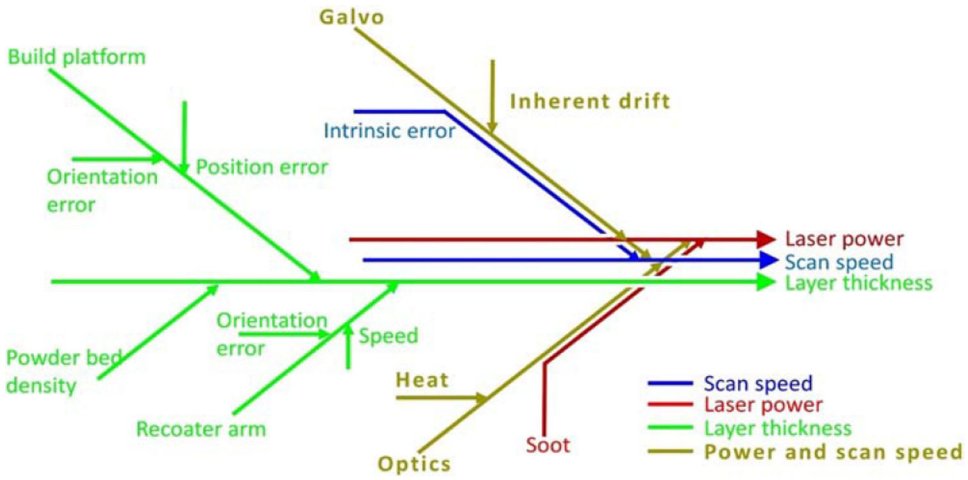

Fig. 5.

Uncertainty sources in a fishbone diagram for laser power, scan speed, and layer thickness

NIST Author Manuscript

NIST Author Manuscript

NIST Author Manuscript

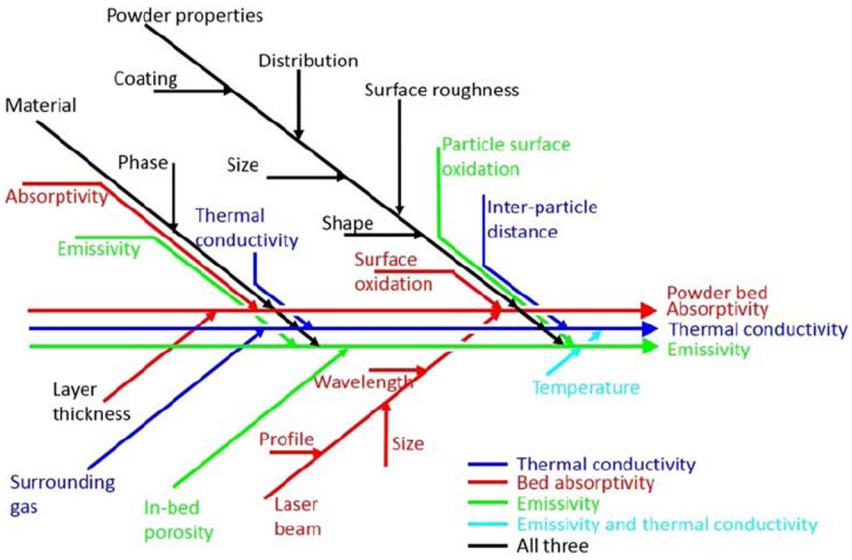

Fig. 6.

Uncertainty sources in a fishbone diagram for powder bed absorptivity, powder bed thermal conductivity, and powder bed emissivity

NIST Author Manuscript

NIST Author Manuscript

NIST Author Manuscript

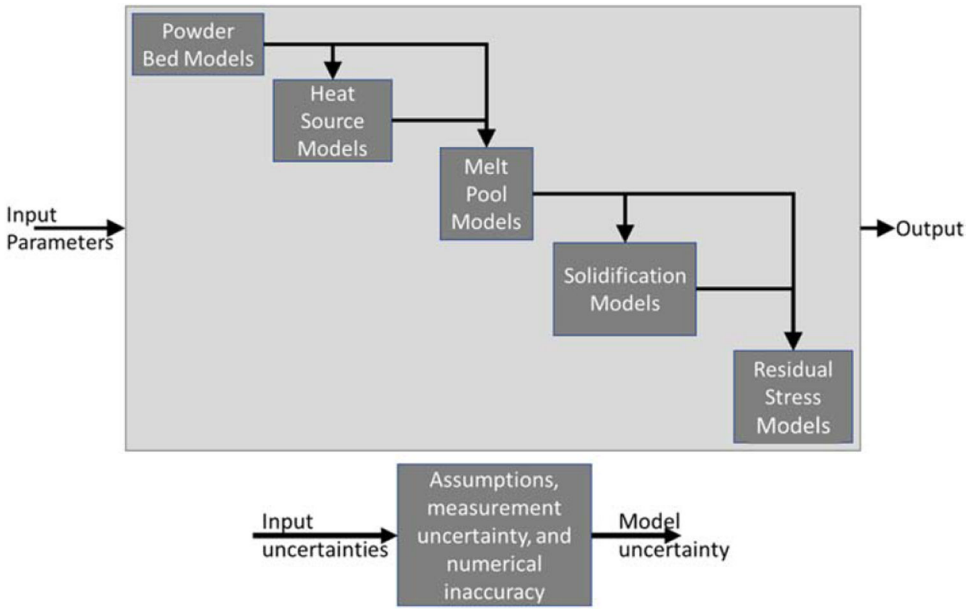

Fig. 7.
Cascading effect of uncertainty in L-PBF

NIST Author Manuscript NIST Author Manuscript NIST Author Manuscript

Table 1

Inputs, outputs, and characteristics of heat source models

Inputs	Methods	Descriptions/assumptions	Outputs
• Powder size, distribution, and shape • Beam power, wavelength, spot size, and scan speed • Density of powder material • Absorptivity of bulk • Thermal conductivity of bulk • Powder bed (continuum or distributed) • Power density distribution (point, cylindrical, ellipsoidal, and Gaussian) • Dimensionality of absorbed energy[a] (surface or volumetric: double ellipsoid, Gaussian, or others [58]) • Optical material properties • Powder bed structure • Layer thickness • Thermal diffusivity of bulk • Specific heat capacity of bulk • Latent heat of fusion • Emissivity of powder surface • Melting temperature • Powder bed absorptivity	Radiation transfer model [51]Ray tracing model [41,42,54,58,59]Beer–Lambert approach[55–57]	• Derived from continuum RTE using powder bed porosity and powder surface area • Assumes small particle size and penetration depth compared to spot size and layer thickness • Ignores scattering from individual particle • Preferable when continuum powder bed is assumed • Not applicable for thin, low-porosity powder layer • Based on principles of geometrical optics • Accounts for the effect of multiple reflections • Tracks position, orientation, trajectory, and power of individual ray • Requires larger powder size compared to wavelength • Captures nonuniform absorptivity in scan track • Detects partially melted particles that cause defects • Uses exponential decay function to relate absorbed energy with penetration depth • Assumes beam power is mainly absorbed by powder surface at first incidence • Does not account for scattering from individual particles • More applicable for continuum powder bed	• Absorbed energy and distribution • Absorptivity coefficient of powder bed • Absorbed energy and distribution

[a]The absorbed energy has to be considered as volumetric instead of surface because in the latter case no model is required [21].

NIST Author Manuscript NIST Author Manuscript NIST Author Manuscript

Table 2

Inputs, outputs, and characteristics of melt pool models

Inputs	Model	Descriptions/assumptions	Outputs
• Thermal conductivity of material • Density of material • Specific heat capacity • Melting temperature • Latent heat of fusion • Laser power • Scan speed • Preheat temperature • Powder bed absorptivity	Rosenthal's based thermal model [45,87]FEM-based thermal model [50,57,74–76,88–92]Lattice Boltzmann method (LBM) [13,56,93]Computational fluid dynamics (CFD) [63–65,79–83, 94–97]	• Uses isotherm migration method • Tracks the location of solidification front • Uses temperature-dependent material properties • Assumes point heat source • Assumes surface energy distribution • Assumes powder bed as continuum body • Uses FEM software: ANSYS, ABAQUS, 3DSIM, etc. to solve heat conduction governing equations and boundary conditions • Volumetric energy distribution can be considered • Assumes continuum powder bed • Ignores the fluid dynamics of the melt pool and associated effects • Simulate the fluid dynamics of melt pool by solving discretized Boltzmann equation on a lattice • Considers individual powder particles • Considers effects of capillary, wetting, Marangoni, recoil pressure, vaporization • Numerically solves mass, momentum, and energy conservation equations using CFD methodologies (FEM, FDM, and/or FVM) coupling with VOF • Utilizes CFD tools like OpenFOAM and Flow-3D • Considers powder bed as distributed particles • Considers effects of capillary, wetting, Marangoni, recoil pressure, and vaporization	• Melt pool width • Melt pool length • Temperature field • Melt pool width • Melt pool length • Melt pool depth • Temperature field • Melt pool width • Melt pool length • Melt pool depth • Surface roughness • Porosity: gas pores, intertrack voids • Layer connection defects • Balling effect and nonuniformity • Keyhole defects
• Laser power • Beam size • Layer thickness • Scan speed • Powder bed absorptivity • Packing density/porosity • Powder bed thermal conductivity • Latent heat of fusion • Density of material • Emissivity • Convection coefficient • Preheat temperature • Solidus and liquidus temperatures • Beam power • Scan speed • Beam size • Layer thickness • Density of material at liquid and solid states • Viscosity • Surface tension coefficient			

NIST Author Manuscript NIST Author Manuscript NIST Author Manuscript

Inputs	Model	Descriptions/assumptions	Outputs
• Gravity • Thermal conductivity of liquid and solid • Specific heat capacity of liquid and solid • Solidus and liquidus temperatures • Boiling temperature • Preheat temperature • Latent heat of fusion and vaporization • Emissivity • Saturated vapor pressure • Powder packing density • Powder bed absorptivity • Temperature coefficient of surface tension • Powder size distribution			